

## EFFECT OF HEATED WALL POSITION ON MIXED CONVECTION IN A CHANNEL WITH AN OPEN CAVITY

*Oronzio Manca and Sergio Nardini*

*Dipartimento di Ingegneria Aerospaziale, Seconda Università di Napoli, Aversa (CE), Italia*

*Khalil Khanafer and Kambiz Vafai*

*Department of Mechanical Engineering, University of California, Riverside, Riverside, California, USA*

*Mixed convection in an open cavity with a heated wall bounded by a horizontally insulated plate is studied numerically. Three basic heating modes are considered: (a) the heated wall is on the inflow side (assisting flow); (b) the heated wall is on the outflow side (opposing flow); and (c) the heated wall is the horizontal surface of the cavity (heating from below). Mixed convection fluid flow and heat transfer within the cavity is governed by the buoyancy parameter, Richardson number ( $Ri$ ), and Reynolds number ( $Re$ ). The results are reported in terms of streamlines, isotherms, wall temperature, and the velocity profiles in the cavity for  $Ri = 0.1$  and  $100$ ,  $Re = 100$  and  $1000$ , and the ratio between the channel and cavity heights ( $H/D$ ) is in the range  $0.1$ – $1.5$ . The present results show that the maximum temperature values decrease as the Reynolds and the Richardson numbers increase. The effect of the  $H/D$  ratio is found to play a significant role on streamline and isotherm patterns for different heating configurations. The present investigation shows that the opposing forced flow configuration has the highest thermal performance in terms of both maximum temperature and average Nusselt number.*

### INTRODUCTION

Mixed convection flow and heat transfer in enclosures is of great interest in engineering and science. This interest stems from its importance in a wide range of engineering areas such as nuclear reactors, solar collectors, crystal growth, and cooling of electronic systems. Due to its simplicity in design and low maintenance cost, air-cooling systems have become a primary cooling medium for electronic systems. The electronic components, which are considered as heat sources, are usually mounted on the vertical boards and the heat generated by these sources is removed by both natural convection and application of an externally induced flow of

Received 19 March 2002; accepted 29 April 2002.

This work was supported by the CNR with grants on Bilateral Research Projects n.97.03198.07 and n.98.00976.07 and MURST under 1999 grant research program Enhancement Techniques in Thermofluids.

Address correspondence to Professor K. Vafai, Dept. of Mechanical Engineering, University of California, Riverside, A363 Bourns Hall, Riverside, CA 92521-0425, USA. E-mail: vafai@enr.ucr.edu



decrease with Rayleigh number. For mixed convection flow in enclosures, Oosthuizen and Paul [6] studied numerically using the Galerkin finite element method mixed convection heat transfer in a cavity with uniformly heated, isothermal vertical walls and horizontal adiabatic walls. They considered the effect of the forced flow, either aiding or opposing, on the buoyancy force. The forced flow was considered to enter and to leave the enclosure across the cold wall. The numerical heat transfer results were obtained for various pertinent controlling parameters of the problem. A similar study was conducted by Simoneau et al. [7] on the interaction between an injection and laminar natural convection in a thermally driven cavity.

A comprehensive study was conducted by Vafai and coworkers [8–12] to investigate basic aspects and physics of the flow field within the open-ended structures and the effect of the extended computational domain on the flow and heat transfer inside the open domain and its immediate surroundings. In these studies, they established that the extent of the enlarged computational domain has a substantially larger effect than previously reported by other investigators.

In this analysis, the forced flow was considered to enter the enclosure through the hot wall and to leave through the opposite cold wall. Both aiding and opposing forced flow cases were investigated here. Papanicolaou and Jaluria [13] studied numerically the mixed convection transport from an isolated heat source with a uniform heat flux input within a rectangular enclosure. Their results showed that the average Nusselt number increases with an increase in the Richardson number at a fixed Reynolds number. Also, an increase in the heat transfer rate was found with an increase in the Reynolds number for a fixed value of Richardson number. Moreover, a rapid increase in heat transfer was observed with an increase in Richardson number when natural convection heat transfer was dominant. Later on, the same authors [14] studied numerically mixed convection from a localized heat source in a cavity with conducting walls. The numerical results showed that the heat transfer from the source was higher if the solid wall thermal conductivity was higher. More recently a numerical study of an enclosure with a heated vertical plate located in the cavity was carried out in [15]. Discrete heat sources were embedded on the plate and different orientations were considered. When the heat source was embedded on the right surface of the board, the value of the convective Nusselt number was found to be independent of the location of the heat source.

Even though the case for a constant heat flux on the horizontal surface exposed to the forced convection has been studied, the case for a constant heat flux on a vertical surface has received little attention. In this work, a cavity located below a channel is considered, as shown in Figure 1. Air flows through the channel. One of the walls of the cavity experiences a uniform heat flux, while the other walls are adiabatic. This produces an interaction between a buoyancy-induced flow and a forced flow. Three resulting cases are investigated: (a) forced flow in the channel assisting the motion due to the natural convection within the cavity; (b) forced flow in the channel opposing the motion due to the natural convection within the cavity; and (c) forced flow in the channel and natural convection due to a heat source over the cavity bottom wall. The results for stream function profiles and temperature distribution are obtained. Also, the heated wall temperature profiles and the velocity profiles in several sections of the cavity are presented.

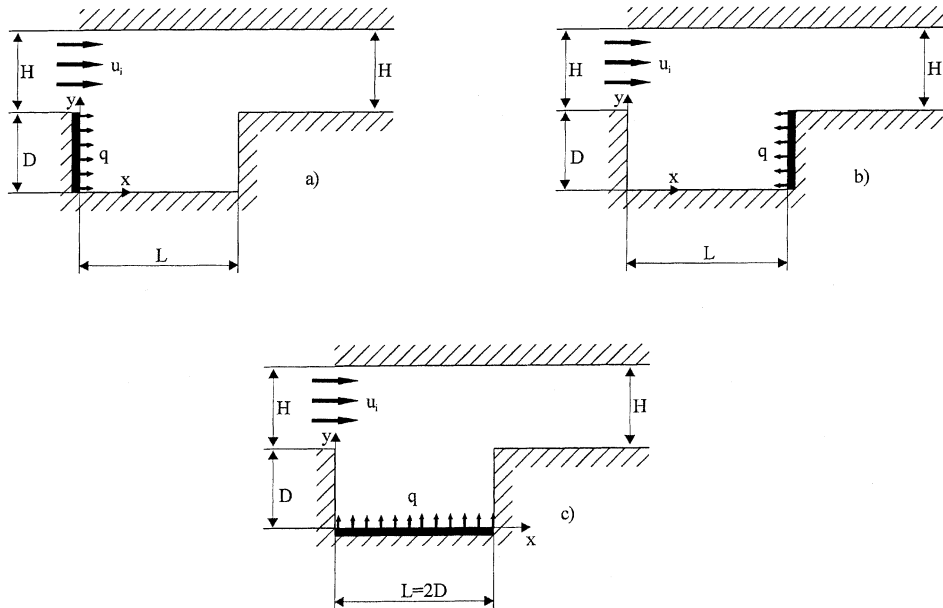


**Figure 1.** Geometry under consideration: (a) assisting forced flow, (b) opposing forced flow, and (c) heating from below.

### PHYSICAL MODEL AND ASSUMPTIONS

The geometry under investigation is shown in Figure 1. One wall of the U-shaped cavity is heated by a uniform heat flux and the other walls are adiabatic. Flow enters through the left opening at a uniform velocity,  $u_i$ . It is assumed that the incoming flow is at an ambient temperature,  $T_i$ , and the outgoing flow is assumed to have zero diffusion flux for all variables (outflow boundary conditions). Flow in the cavity is assumed to be two-dimensional, laminar, and incompressible with negligible viscous dissipation. All the thermophysical properties of the fluid are assumed constant except for the variation in density with temperature (Boussinesq approximation) giving rise to the buoyancy forces. The thermophysical properties of the fluid are evaluated at the ambient temperature,  $T_i$ , which is equal to 300 K in all cases.

Taking into account the above-mentioned assumptions, we can write in non-dimensional form the governing equations for this investigation, with constant thermophysical properties and Boussinesq approximation:

$$\frac{\partial U}{\partial X} + \frac{\partial V}{\partial Y} = 0 \quad (1)$$

$$U \frac{\partial U}{\partial X} + V \frac{\partial U}{\partial Y} = -\frac{\partial P}{\partial X} + \frac{1}{\text{Re}} \left( \frac{\partial^2 U}{\partial X^2} + \frac{\partial^2 U}{\partial Y^2} \right) \quad (2)$$

$$U \frac{\partial V}{\partial X} + V \frac{\partial V}{\partial Y} = -\frac{\partial P}{\partial Y} + \frac{1}{\text{Re}} \left( \frac{\partial^2 V}{\partial X^2} + \frac{\partial^2 V}{\partial Y^2} \right) + \frac{\text{Gr}}{\text{Re}^2} \theta \quad (3)$$

$$U \frac{\partial \theta}{\partial X} + V \frac{\partial \theta}{\partial Y} = \frac{1}{\text{Pr Re}} \left( \frac{\partial^2 \theta}{\partial X^2} + \frac{\partial^2 \theta}{\partial Y^2} \right) \quad (4)$$

where  $\text{Re} = u_i D / \nu$  is the Reynolds number,  $\text{Gr} = g \beta_T q D^4 / \nu^2 k$  is the Grashof number, and  $\text{Pr} = \nu / \alpha$  is the Prandtl number. The Richardson number is defined as  $\text{Ri} = \text{Gr} / \text{Re}^2$ .

Equation (1)–(4) were cast in nondimensional form by using the following nondimensional variables:

$$\left. \begin{aligned} X &= \frac{x}{D} & Y &= \frac{y}{D} & \theta &= \frac{T - T_i}{(qD/k)} \\ U &= \frac{u}{u_i} & V &= \frac{v}{u_i} & P &= \frac{pH}{\mu u_i} \end{aligned} \right\} \quad (5)$$

In the above equations,  $D$  is the height of the vertical heated wall,  $\beta_T$  is the volumetric expansion coefficient,  $p$  is the fluid pressure,  $q$  is the heat flux,  $u$  and  $v$  are the velocity components in the  $x$ - and  $y$ -directions,  $T$  is the fluid temperature, and  $T_i$  is the inflow temperature.

The average Nusselt number is

$$\text{Nu} = \frac{1}{L_H} \int_0^{L_H} \text{Nu}(r) dr = \frac{1}{L_H} \int_0^{L_H} \frac{h(r)r}{k} dr \quad (6)$$

with

$$h(r) = \frac{q}{T_w(r) - T_i} \quad (7)$$

where  $L_H$  is the length of the heated wall and  $r$  is either the  $x$ - or  $y$ -coordinate depending on the location of the heated wall.

## NUMERICAL SCHEME

The numerical procedure used in this work is based on the Galerkin weighted residual method of finite element formulation. The application of this technique is well described by Taylor and Hood [16] and Gresho et al. [17] and its application is well documented [18]. The segregated solution method was chosen to solve the governing equations, which were linearized implicitly with respect to the equation's dependent variable. The advantage of using this method is that the global system matrix is decomposed into smaller submatrices and then solved in a sequential manner. This approach will result in substantially fewer storage requirements. The conjugate residual scheme is used to solve the symmetric pressure-type equation systems, while the conjugate gradient squared is used for the nonsymmetric advection-diffusion-type equations. A variable grid size system is implemented in the

**Table 1.** Comparison of results for validation at  $Pr = 0.7$ ,  $Re = 100$ ,  $Ri = 1$ 

	Present	Ref. [14]
Nu	3.06	3.13
$\theta_{\max}$	3.34	3.56
$\Psi_{\max}$	1.38	1.37

present investigation especially near the walls to capture the rapid changes in the dependent variables. The following enforced convergence criterion is implemented in this study to ensure the convergence of the dependent variables:

$$\frac{\|\Lambda^{n+1} - \Lambda^n\|_{\infty}}{\|\Lambda^{n+1}\|_{\infty}} \leq 10^{-5} \quad (8)$$

where  $\Lambda$  is the dependent variable and  $n$  is the iteration index.

This numerical model was validated by solving the configuration investigated in [8, 9]. The comparison is presented in Table 1 in terms of the average Nusselt number, dimensionless maximum temperature on the heated strip, and dimensionless maximum stream function. The percentage differences between the global values are in very good agreement, whereas a weak discrepancy is observed for  $\theta_{\max}$ .

Preliminary results were obtained to inspect the field variables grid-independency solutions. In Figure 2 streamlines and temperature fields are presented for  $Re = 1000$ ,  $Ri = 100$ , and for three different nonuniform grid systems with the following number of nodes in the U-shaped cavity:  $30 \times 30$  (Figure 2a),  $50 \times 50$  (Figure 2b),  $70 \times 70$  (Figure 2c), and  $90 \times 90$  (Figure 2d). As shown in Figure 2 with respect to the minimum and maximum values of the field variables, adequate results can be achieved using nonuniform node points of  $70 \times 70$ . Additional refinement of node points did not render any appreciable improvement in the results. As an additional check on the accuracy of the present grid system, temperature and velocity component profiles along the horizontal midsection of the cavity ( $Y = D/2$ ) are illustrated in Figure 3. The temperature and the velocity profiles for  $50 \times 50$  and  $70 \times 70$  grid systems are very similar as depicted in Figure 3. To test the required outlet channel length, the streamlines and the temperature distribution for  $Re = 1000$  and  $Ri = 100$  and for four different lengths of the outlet channel,  $L_{\text{exit}} = L$ ,  $2L$ ,  $3L$ , and  $4L$  are reported in Figure 4. No differences are observed between the maximum and the minimum values of the streamlines and the isotherms. Based on the above observations, numerical runs are carried out employing a computational domain with  $L_{\text{exit}} = 4L$  and a non uniform grid with a number of nodes equal to  $70 \times 70$  for the bottom cavity (U-shaped) in order to obtain a good resolution and a reasonable computational runtime. The analysis was carried out for the following three classes of configurations: (a) the left wall is heated and the forced flow assists the motion due to the natural convection in the cavity; (b) the right wall is heated and the forced flow opposes the motion due to the natural convection in the cavity; and (c) the bottom wall is heated.

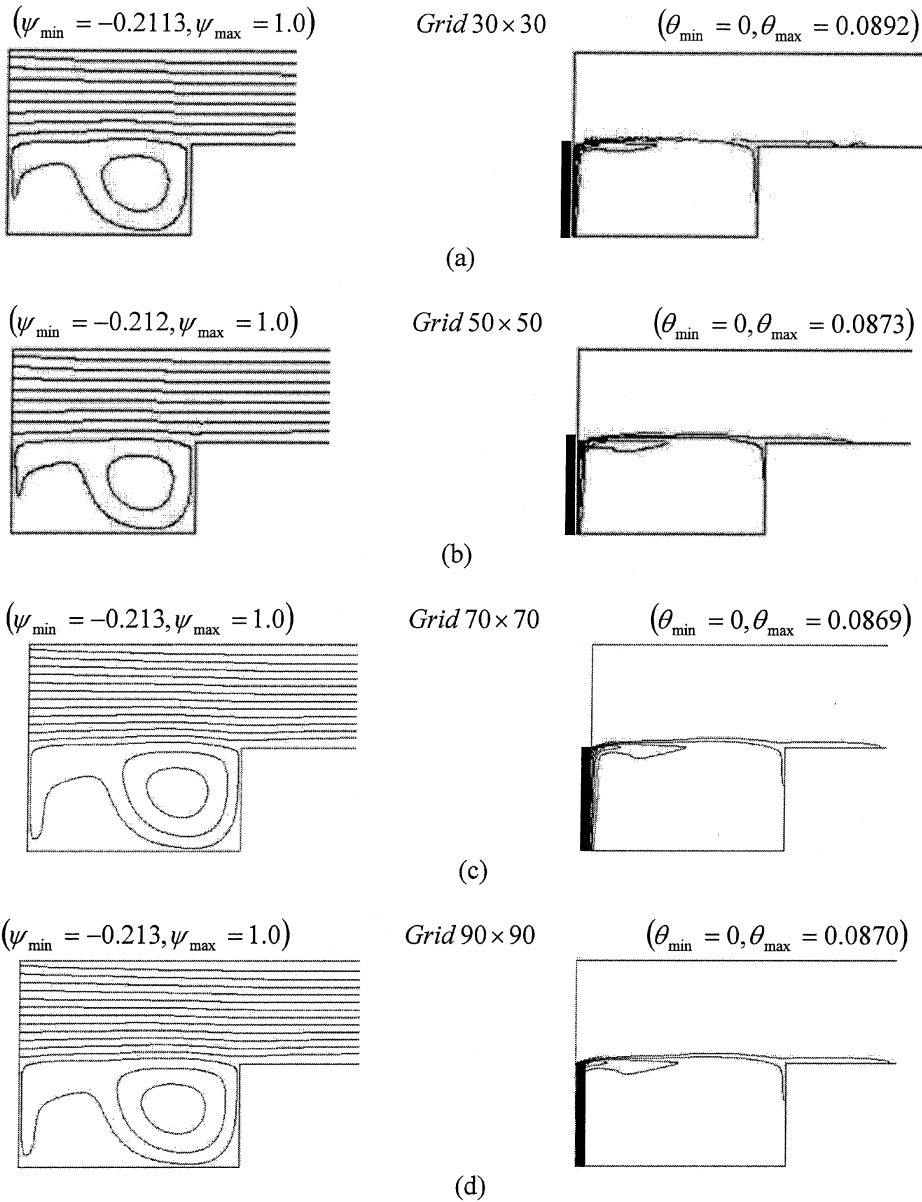


**Figure 2.** Assisting forced flow,  $H/D = 1.0$ ,  $Re = 1000$ , and  $Ri = 100$ : (a)  $30 \times 30$  nodes; (b)  $50 \times 50$  nodes; (c)  $70 \times 70$  nodes; and (d)  $90 \times 90$  nodes.

## RESULTS AND DISCUSSION

The results presented here were for a U-shaped cavity with an aspect ratio  $L/D$  of 2. The ratio of the height of the inflow and outflow openings to the heat source length  $H/D$  was equal to 0.1, 1, and 1.5. The Reynolds numbers investigated were

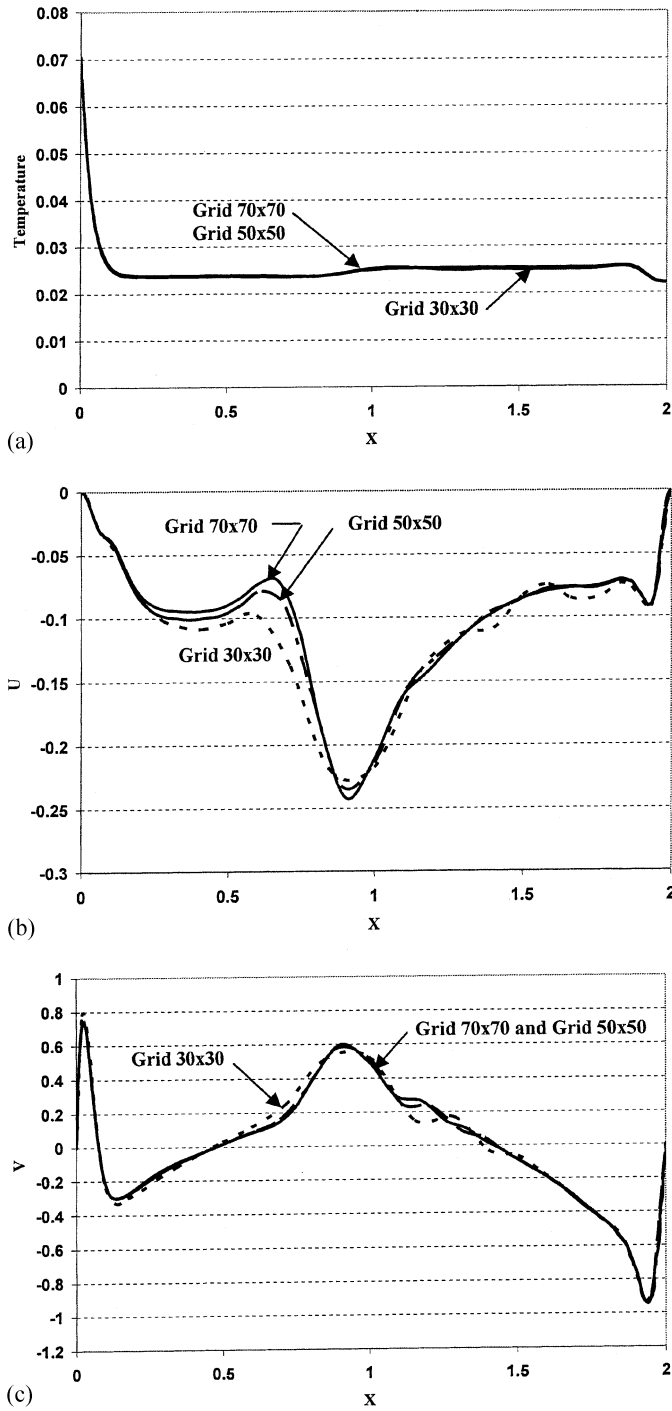


**Figure 3.** Effect of the number of mesh nodes for assisting forced flow,  $H/D=1.0$ ,  $Re=1000$ , and  $Ri=100$ , at the horizontal midplane: (a) on the dimensionless temperature; (b) horizontal velocity component at the horizontal midplane; and (c) vertical velocity component.

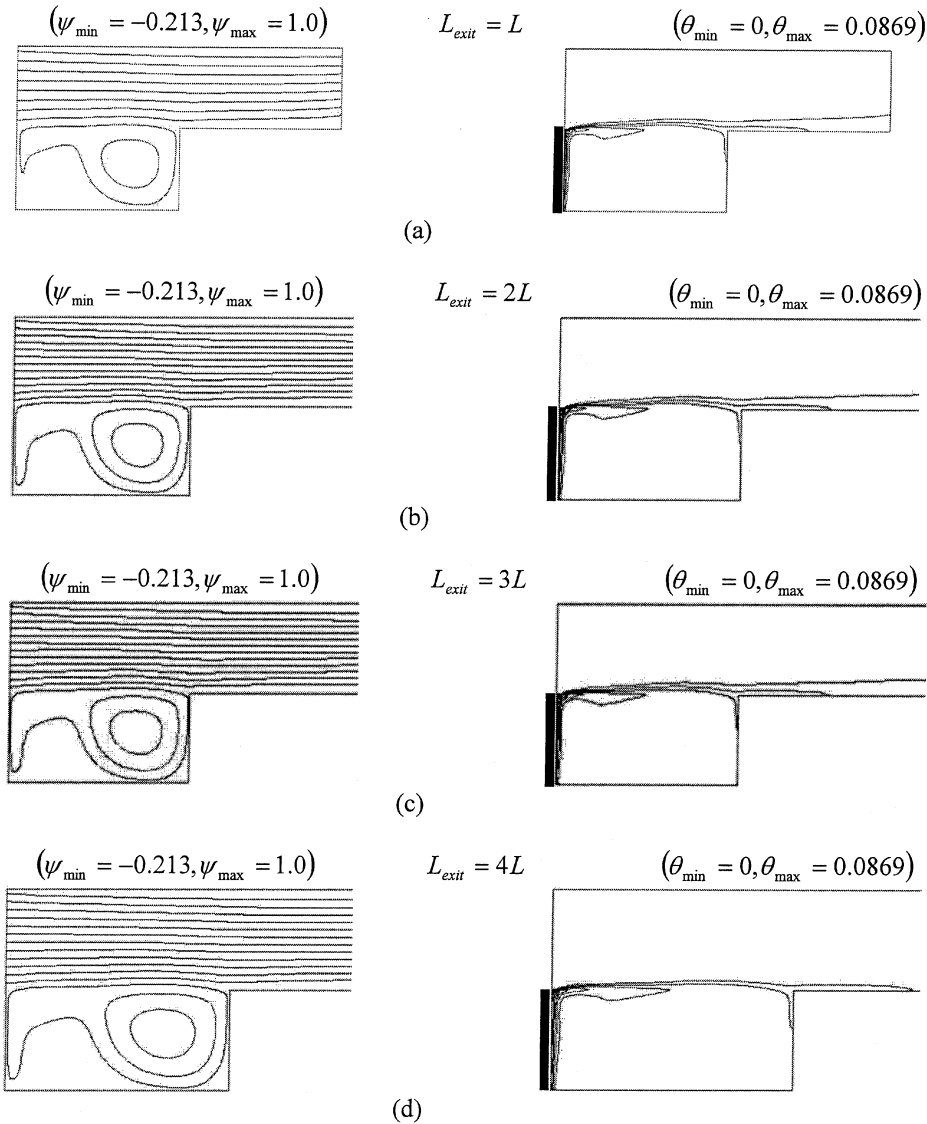


**Figure 4.** Assisting forced flow,  $H/D=1.0$ ,  $Re=1000$ , and  $Ri=100$ : (a)  $L_{exit}=L$ ; (b)  $L_{exit}=2L$ ; (c)  $L_{exit}=3L$ ; and (d)  $L_{exit}=4L$ .

100 and 1000; these are in the laminar regime. At each of these  $Re$  values,  $Ri = Gr/Re^2$  values of 0.1 and 100 were used. Computation was carried out for the three configurations. For  $Re=1000$  and  $Ri=0.1$  an oscillatory behavior was observed similar to the one noticed in [13] for similar values of  $Re$  and  $Ri$ .

In the following, several cases related to the three configurations are compared in terms of streamlines, isotherms, heated wall temperatures, and velocity components. Figure 5 shows the streamlines and the isotherms for assisting forced flow for different Richardson numbers at  $Re = 100$ . For relatively small values of

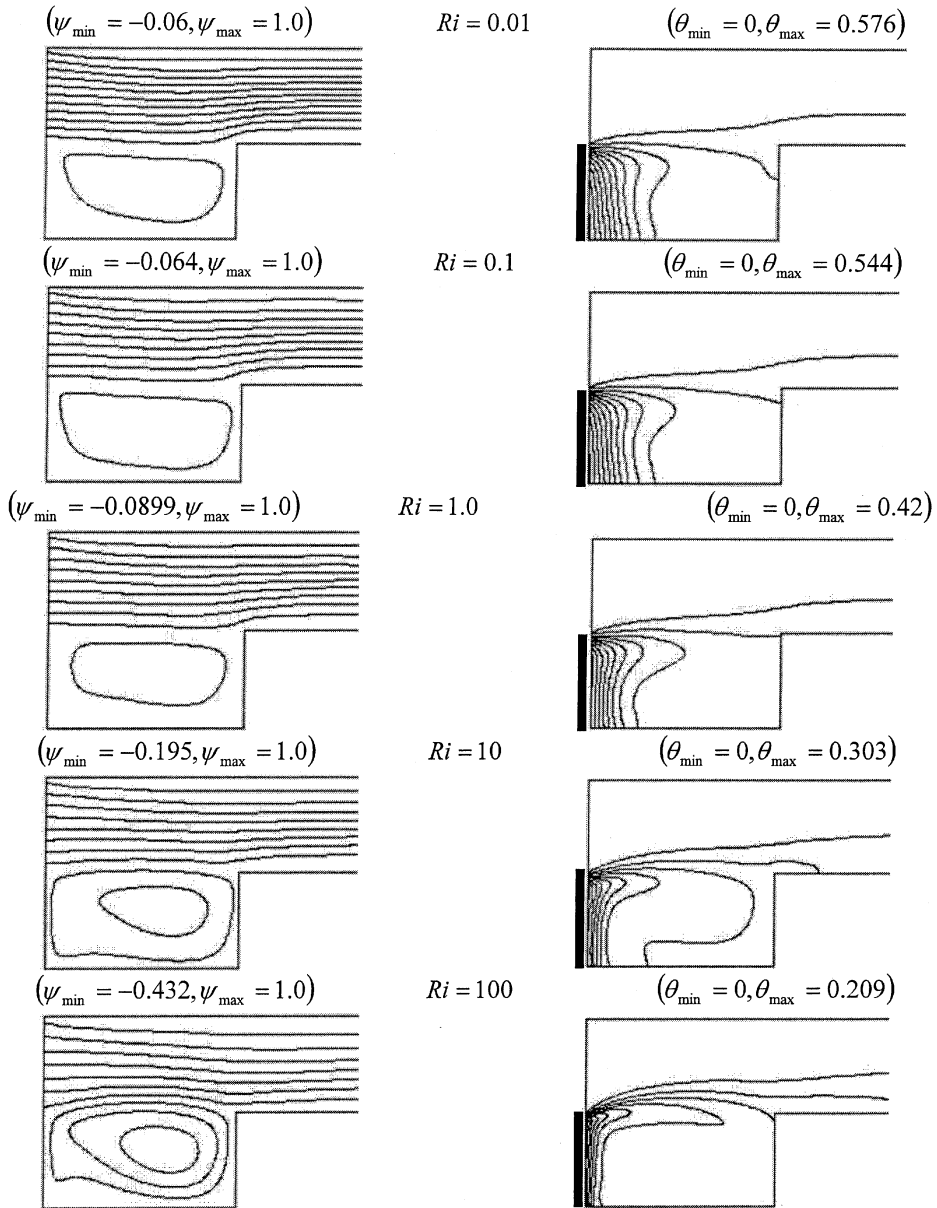


**Figure 5.** The effect of the Richardson number on the streamlines and the isotherms for assisting forced flow ( $H/D = 1$ ,  $Re = 100$ ).

Richardson number ( $Ri \ll 1$ ), a small recirculating cell is present in the open cavity and the heat transfer between the heat source and the externally induced airflow is provided mainly by heat conduction. This is because the buoyancy effect is overwhelmed by the mechanical effect of the externally induced flow. As the Richardson number increases, as shown in Figure 5, the intensity of the main

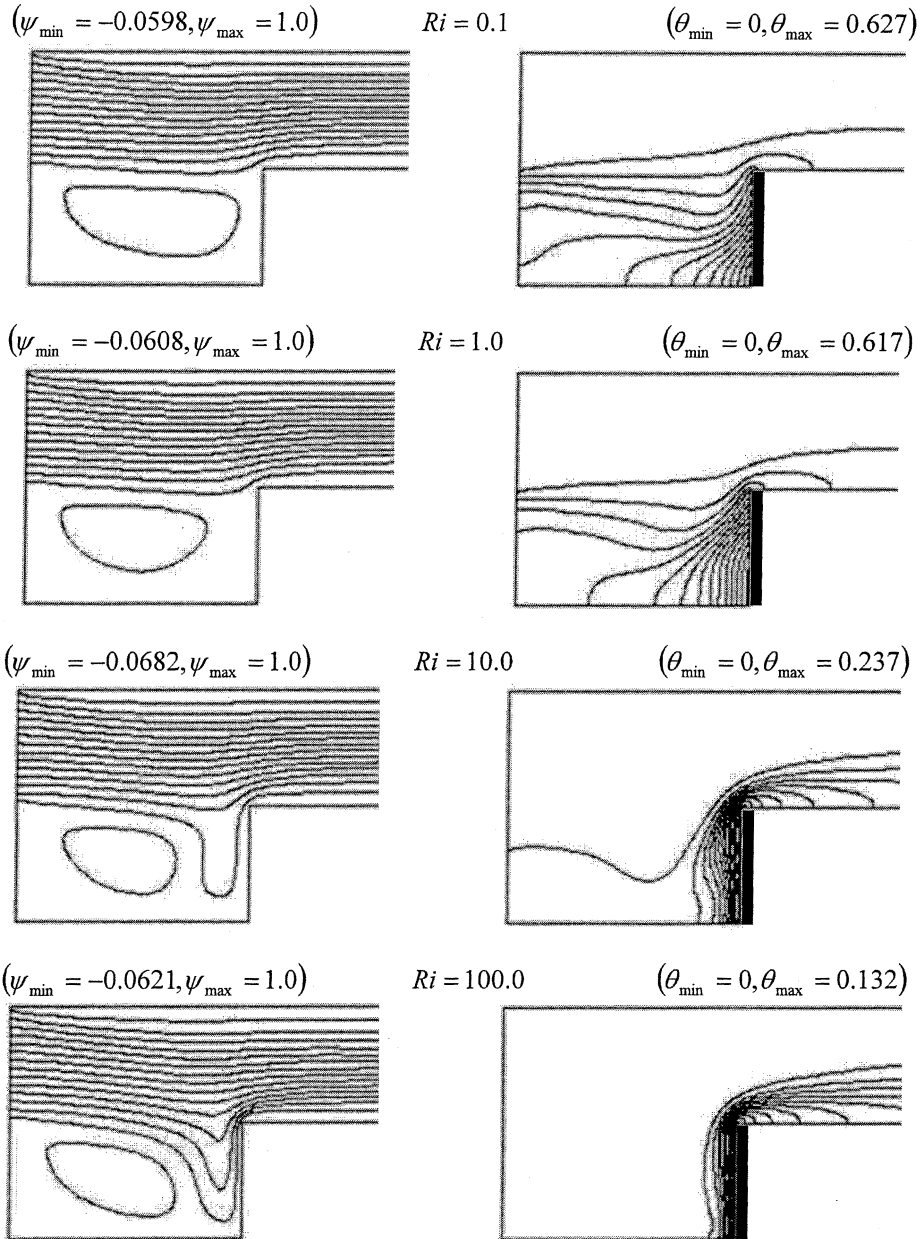
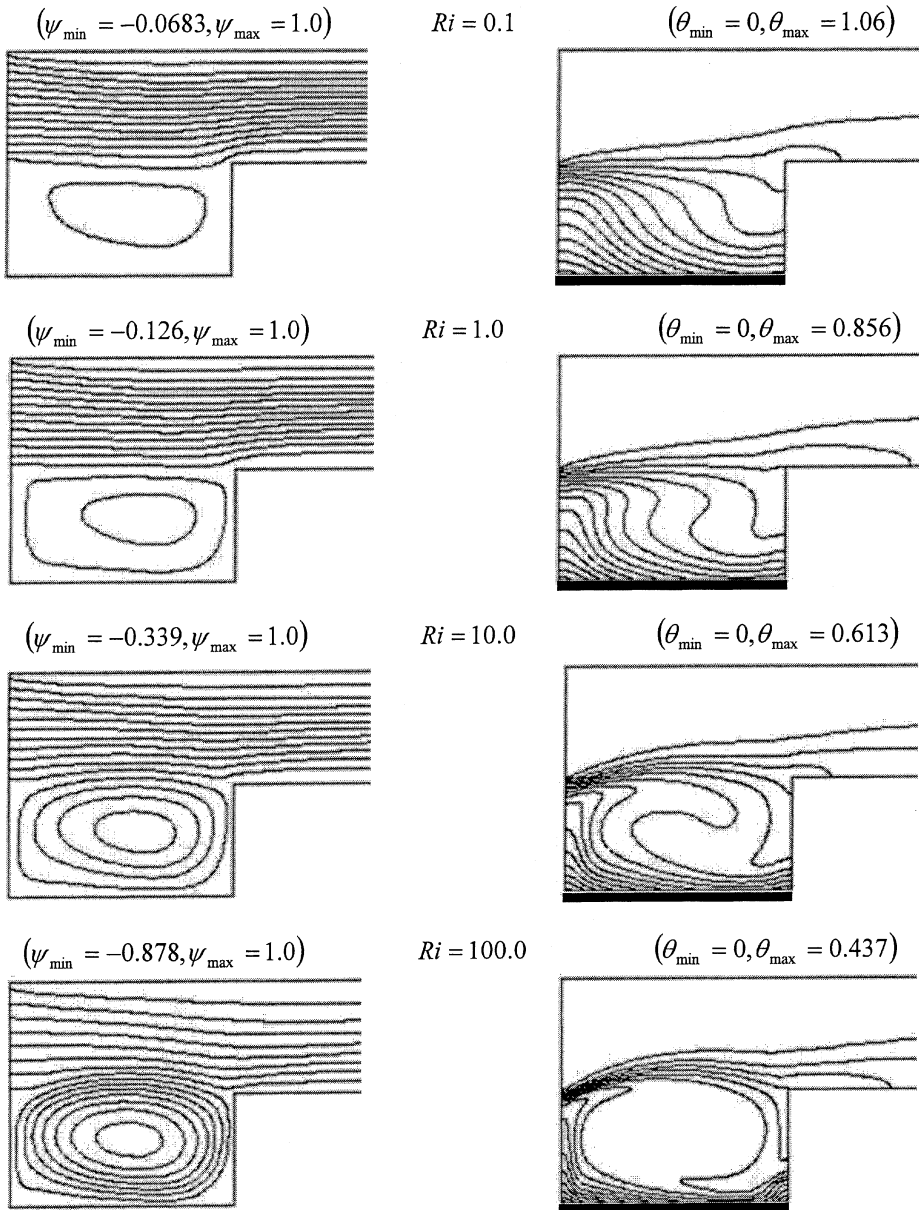


Figure 6. The effect of the Richardson number on the streamlines and the isotherms for opposing forced flow ( $H/D = 1$ ,  $Re = 100$ ).

circulation increases and fills the entire enclosure. As seen in Figure 5, the region affected by the heat source is quite small for small Richardson numbers since the induced flow does not mix with the fluid inside the enclosure. Moreover, the isotherms show that the temperature distribution is nearly uniform with respect to the Y coordinate except close to the induced flow, indicating that most of the heat transfer is carried out by conduction. For a higher Richardson number ( $Ri = 100$ ), the buoyancy effects are much stronger and result in a more vigorous loop in the enclosure as depicted in Figure 5. Also, the formation of a plume becomes more pronounced at a higher Richardson number. Figure 5 shows two different regions within the enclosure. The upper part of the enclosure is characterized by almost stratified isotherms, indicating that the heat is transferred from the recirculating flow to the externally induced flow by diffusion. The isotherms within the remaining region are clustered close to the heated wall, which points to the existence of a steep temperature gradient. For the opposing forced flow and  $Ri = 0.1$ , as shown in Figure 6, a weak recirculating cell is present in the enclosure. In addition, the forced flow does not penetrate much in the cavity, exiting next to the upper corner of the heat source. Higher temperature gradients are present in the region close to the lower part of the heat source as shown in Figure 6 ( $Ri = 0.1$ ). As the Richardson number increases to 100, the plume becomes stronger and part of the forced flow is drawn into the cavity. For this case, the maximum temperature at the lower part of the heat source is lower than the maximum temperature for the case where  $Ri = 0.1$ . This can be attributed to the effect of the external airflow penetration into the cavity, which lowers the temperature.

The heating from below is considered in Figure 7 for various Richardson numbers. For  $Ri = 0.1$ , the streamlines are very similar to those reported in Figures 5 and 6, and this is due to the fact that the buoyancy effect is overwhelmed by the effect of the external airflow. In this configuration the forced flow prevails again over the buoyancy effect. The recirculating cell has very low velocity values in the zone adjacent the lower heated wall for small values of Richardson numbers as shown in Figure 7. As in previous cases, the heat transfer between the forced and recirculating flows is merely conductive. The isotherms for  $Ri = 0.1$  are nearly parallel to the horizontal wall. This shows a vertical stratification inside the enclosure, indicating a dominant heat conduction mechanism. For a higher Richardson number value of  $Ri = 100$ , the streamlines in Figure 8 show a nearly symmetrical recirculating cell except close to the lower corners. For this case, the velocity values are higher and the convective currents are stronger. As a consequence, heat removal is much more effective than in the case of  $Ri = 0.1$ .

Figures 8 through 9 show the streamlines and the isotherms for Richardson number between 0.1 and 100 and Reynolds number of 1000 for the assisting case, Figure 8, and for the case with the heated bottom wall, Figure 9. It is noticed in Figure 8 that the recirculating cell in the cavity is adjacent to the insulated vertical wall and the rest of the cavity is at rest. Furthermore, the isotherms are accumulated in the regions close to the heat source and the heat diffusion is predominant for small Richardson number ( $Ri = 0.1$ ) as shown in Figure 8. As the Richardson number increases ( $Ri = 100$ ), the heat removal improves because the convective effects are stronger as shown in Figure 8. For higher Richardson number, the streamlines are clustered near the insulated vertical wall of the enclosure. As a result, high velocity



**Figure 7.** The effect of the Richardson number on the streamlines and the isotherms for heating from below ( $H/D = 1, Re = 100$ ).

gradients are encountered at the vertical wall, indicating a very thin hydrodynamic boundary layer. Also, a small eddy is formed at the lower right corner of the enclosure due to an increase in the Reynolds number that implies a stronger forced flow effect. The isotherms are also clustered in a zone close to the heated wall for higher Richardson numbers, which indicates higher heat transfer by convection. When the lower horizontal wall is heated, Figure 9, the streamlines are very similar

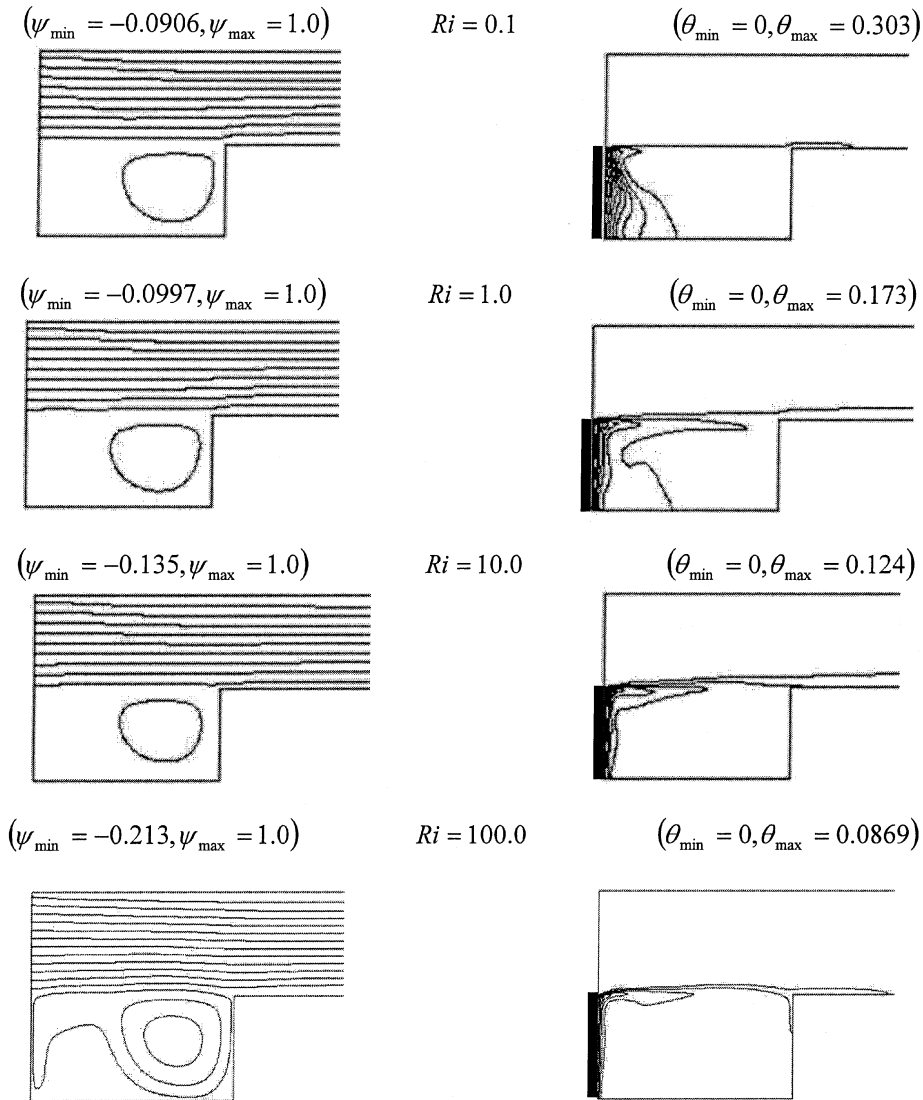


**Figure 8.** The effect of the Richardson number on the streamlines and the isotherms for assisting forced flow ( $H/D = 1$ ,  $Re = 1000$ ).

to those of the assisting case for small Richardson numbers (Figure 8). The recirculating cell allows heat removal at the channel exit section, whereas in the other cavity zone heat removal is merely diffusive because the fluid is nearly motionless in the cavity. The isotherms in Figure 9 highlight this situation. When the Richardson number increases ( $Ri = 100$ ), Figure 9, the main circulation fills the entire cavity and minor cells are visible near the bottom corners.

In Figure 10, the profiles of the heated wall temperature and the vertical velocity component  $V$  for the assisting and opposing forced flows along the  $X$  coordinate at various heights within the enclosure ( $Y = 0.25, 0.50, 0.75$ ) are pre-

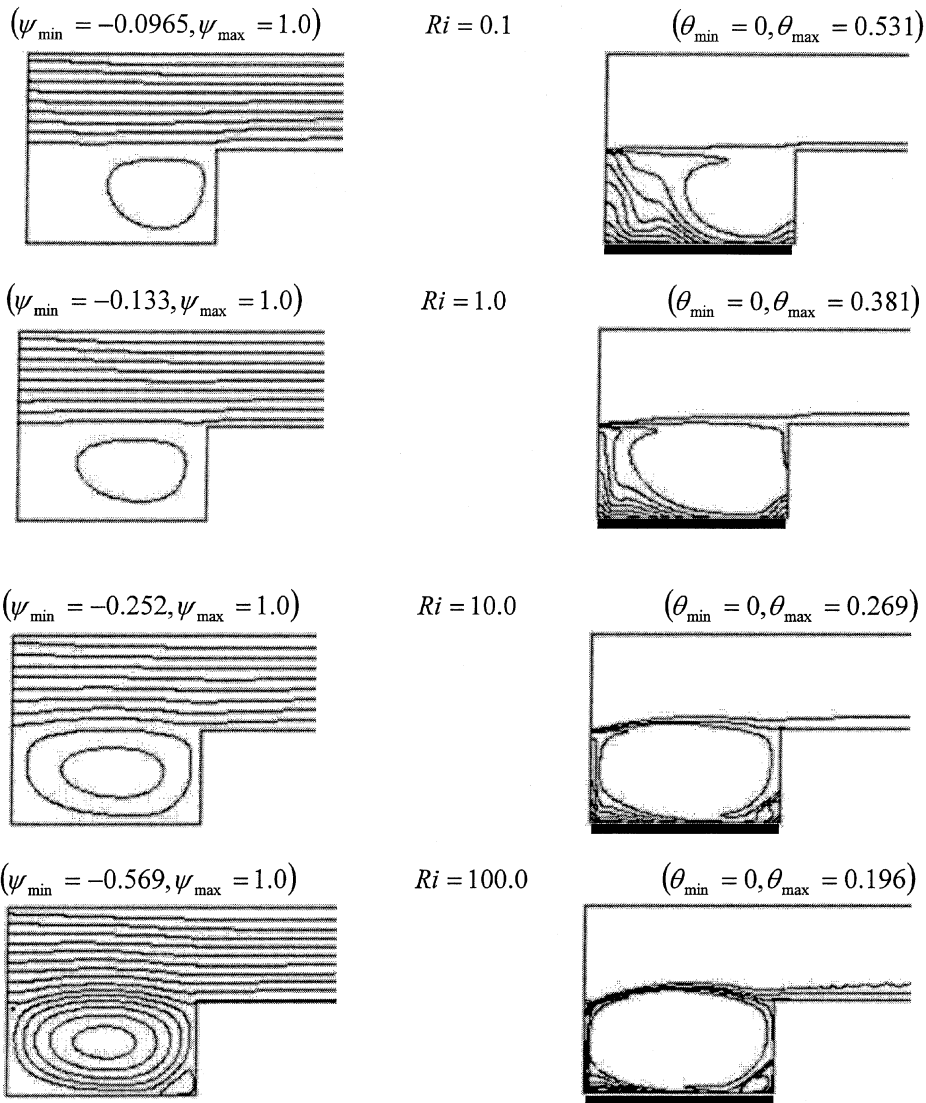
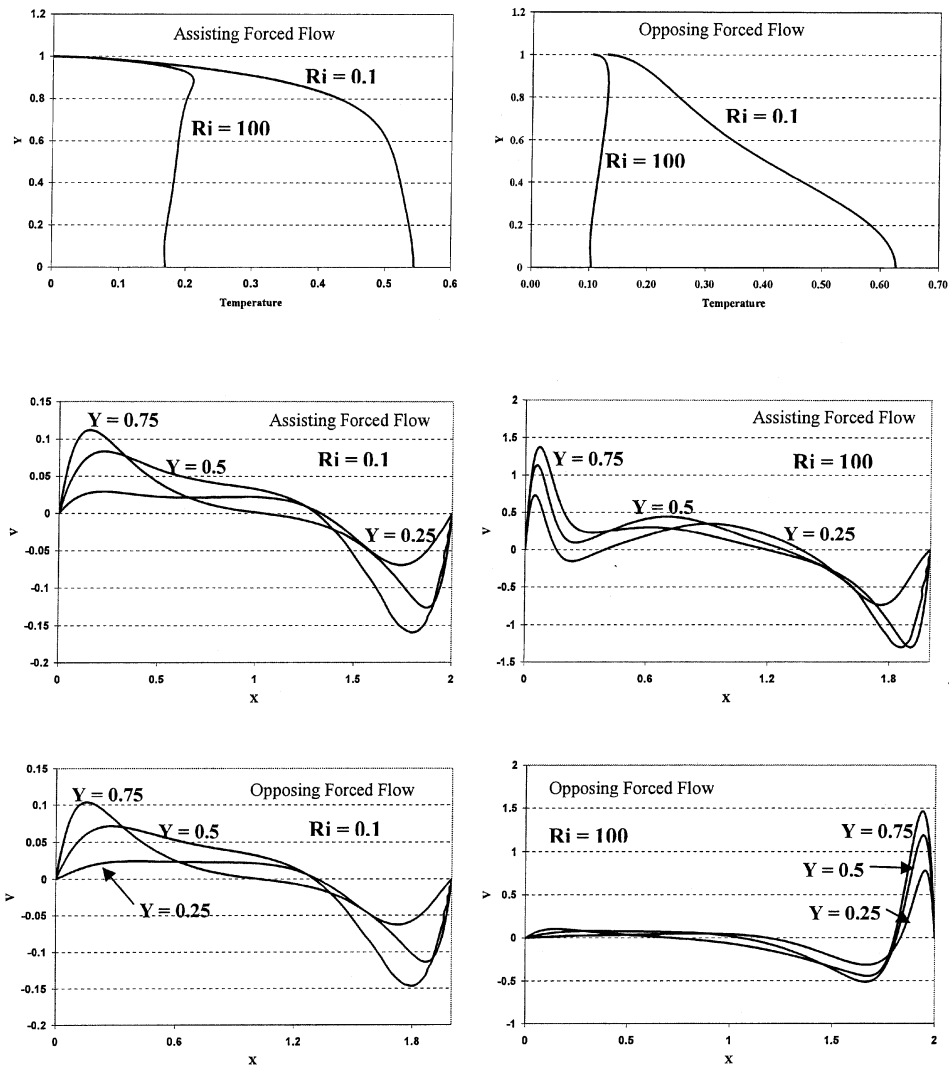


Figure 9. The effect of the Richardson number on the streamlines and the isotherms for heating from below ( $H/D = 1, Re = 1000$ ).

sented for a Reynolds number of 100 and for Richardson numbers of 0.1 and 100, respectively. For assisting forced flow and  $Ri = 0.1$ , Figure 10 shows that the non-dimensional wall temperature has a sharp increase close to the top corner. The maximum value of the temperature is reached close to the cavity bottom wall. Furthermore, the temperature profile is nearly uniform for  $0 < Y < 0.6$ . For opposing forced flow, the nondimensional wall temperature is higher than the one for the assisting case close to the top corner. In addition, the temperature increases gradually and almost linearly between  $Y = 0.9$  and  $0.1$ . The maximum wall temperature



**Figure 10.** Comparison of the temperature and velocity profiles between assisting and opposing forced flows at midsections of the enclosure and various Richardson numbers ( $H/D = 1$ ,  $Re = 100$ ).

value is attained in the lower part of the heated wall because the loop moves from the top to the bottom of the cavity. As the Richardson number increases ( $Ri = 100$ ), for the assisting forced flow, the temperature gradient is again larger close to the top corner, which is adjacent to the inlet opening. However, in this case the maximum temperature value is attained in the upper part of the wall. When  $Re$  increases to 1000, for the assisting forced flow and  $Ri = 0.1$ , the maximum wall temperature is attained near the middle of the heated wall. Furthermore, the profile is much less uniform than the profile for  $Re = 100$ .

The vertical velocity component at various vertical locations is shown in Figures 10 and 11. In Figure 10 and for the assisting forced flow, as the Richardson

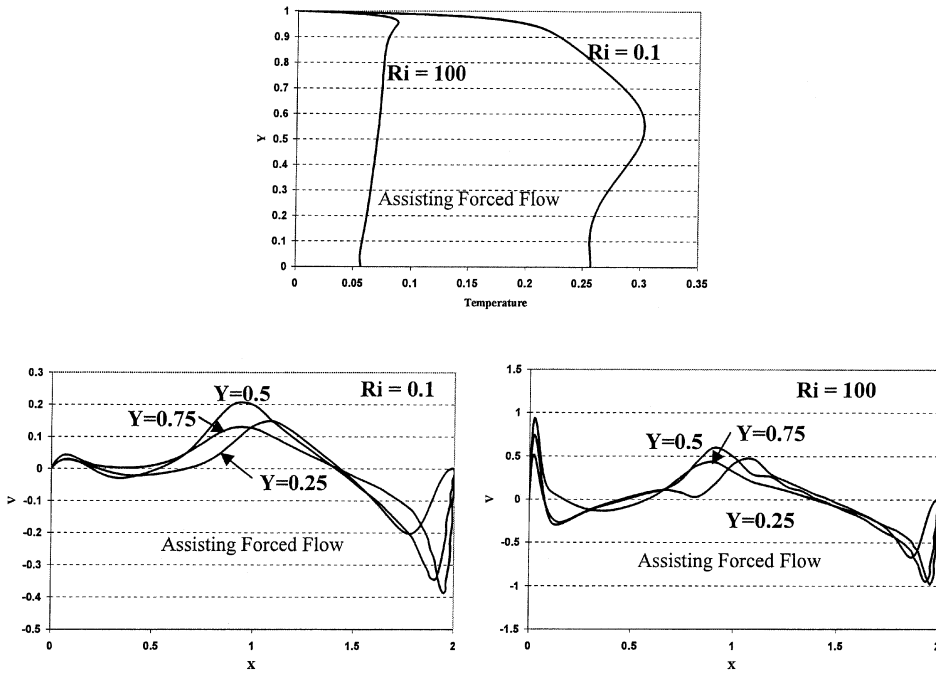


**Figure 11.** Comparison of the temperature and velocity profiles for assisting forced flow at midsections of the enclosure and for various Richardson numbers ( $H/D = 1$ ,  $Re = 1000$ ).

number increases the hydrodynamic boundary layer is well established and the velocity gradients become steeper at both vertical sides of the enclosure. For a small value of the Richardson number, the peak of the velocity profile is almost flat, indicating only a residual buoyancy effect. For the opposing forced flow, as the Richardson number increases to 100 the velocity component is almost zero except near the heat source where the externally induced flow penetrates into the cavity. Also, it can be seen from this figure that a high speed vertical flow occurs near the heat source, indicating a very thin boundary layer region. For a higher Reynolds number ( $Re = 1000$ ), Figure 11 shows the variation of the vertical velocity component at various Richardson numbers for assisting a forced flow scenario. It can be seen from this figure that the values of the vertical velocity component are greater than for  $Re = 100$ . This is because a higher Reynolds number implies faster externally induced airflow, and as a result the vertical velocity component will increase. As the Richardson number increases for the assisting forced flow, the velocity profiles experience a sharp change in the slope at both vertical sides of the enclosure. Also, the velocity at these locations inside the cavity is no longer at rest, similar to the low Reynolds number case.

The effect of varying the ratio of the inflow opening to the height of the vertical heated wall ( $H/D$ ) is shown in Figure 12 through 14 for  $Re = 100$  and  $Ri = 0.1$ . Figure 12 shows the influence of this ratio on the streamlines and the isotherms for assisting forced flow configuration. For  $H/D = 0.1$ , Figure 12 points out the presence of a recirculating cell adjacent to the unheated vertical wall, which occupies

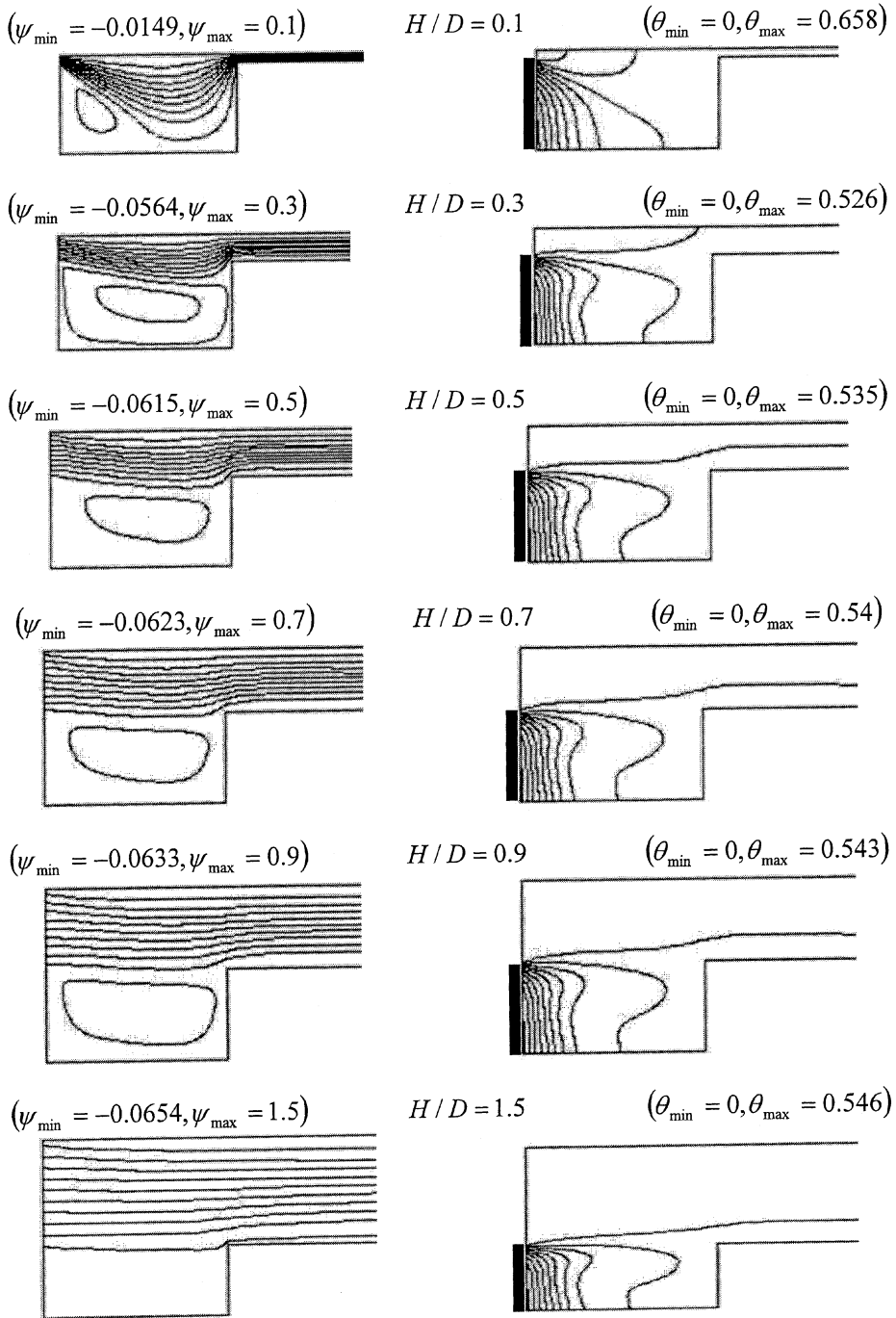


**Figure 12.** Streamlines and isotherms for assisting forced flow at various  $H/D$  ( $Ri = 0.1, Re = 100$ ).

most of the cavity. In addition, a single low speed vortex exists in the zone close to the heated wall. It can be seen from this figure that as the  $H/D$  ratio increases, the behavior of the flow changes essentially from a wall-jet-type flow to an open cavity flow type. For a wall-jet-type flow, the maximum temperature value is  $\theta_{\max} = 0.658$ . The added pressure rise along the channel causes the flow to decelerate along the upper wall and downward displacement of the streamlines in the cavity. As the  $H/D$  ratio increases, the maximum temperature value decreases ( $H/D = 0.3$ ) due to the circulating flow cell within the cavity, which fills the entire region as depicted in this figure. This behavior allows the heat to be carried out by the circulating flow within the cavity (clockwise). In addition, the intensity of the main circulation with the enclosure increases, which causes better heat transfer enhancement. As the  $H/D$  ratio increases further ( $H/D > 0.3$ ), the streamlines and the isotherms patterns remain almost unchanged. This is because the main bulk fluid flows through the channel and not into the cavity as a result of the dominant pressure drop in the channel compared with the added pressure rise in the expansion section.

In the opposing forced flow configuration, Figure 13, the streamlines distribution is similar to those for the assisting forced flow configuration. For  $H/D = 0.1$ , this case represents a jet-wall-type flow, and the maximum temperature value is the lowest for this situation. This is because the main flow penetrates into the cavity, exiting adjacent to the upper corner of the heat source. As the  $H/D$  ratio increases, the maximum temperature value increases significantly (up to  $H/D = 0.5$ ) and then remains nearly constant. This can be attributed to the countereffect of the buoyancy force against the induced airflow, which causes an increase in the maximum temperature values. Moreover, the warmer zone is close to the right lower corner, and this is due to the effect of the recirculating flow within the cavity (clockwise), which opposes the effect of the buoyancy effect. As the  $H/D$  ratio increases further ( $H/D > 0.5$ ), the streamlines and the isotherms patterns almost remain unaltered.

When the cavity is heated from below, Figure 14, the streamlines are similar to the ones for the assisting and opposing forced flows. For  $H/D = 0.1$ , the isotherms are almost symmetrical about the vertical axis of the cavity. Moreover, the isotherms cluster along the horizontal heated wall and the maximum temperature value for this case ( $\theta_{\max} = 0.864$ ) is lower than the one for  $H/D = 1$  ( $\theta_{\max} = 1.06$ ). This is associated with higher temperature gradients in the vertical direction of the enclosure for the case of  $H/D = 0.1$  than the one for  $H/D = 1$ . As the  $H/D$  ratio increases, the main flow penetration decreases and there is no longer symmetrical behavior of the isotherms. In addition, the isotherms in the lower part of the cavity are almost parallel to the horizontal heated wall except at a region adjacent to the right vertical wall (above the middle of the right vertical wall) where the effect of the forced flow is appreciated.

Figures 15 and 16 illustrate the values of the maximum wall temperature and the average Nusselt number as a function of the  $H/D$  ratio for the three considered configurations and  $Re = 100$ . It can be seen from Figure 15 that the maximum nondimensional temperature has higher values for the case of heating from below at various values of the  $H/D$  ratio. In addition, Figure 15 shows for all configurations that variations of  $H/D$  ratio are less significant for ratios greater than 0.4. The effect of varying  $H/D$  ratio on the average Nusselt number is shown in Figure 16. This

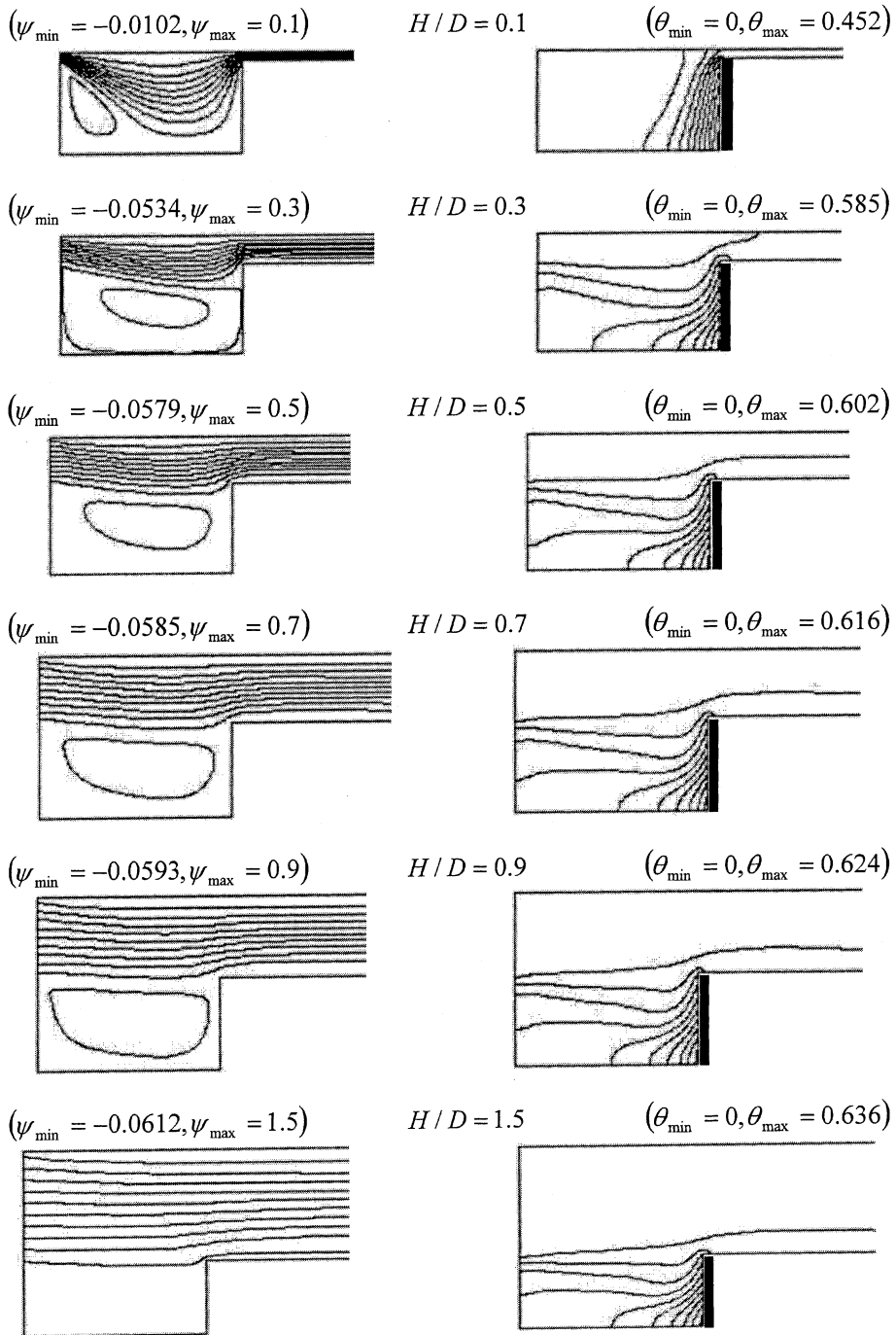


Figure 13. Streamlines and isotherms for opposing forced flow at various  $H/D$  ( $Ri = 0.1, Re = 100$ ).

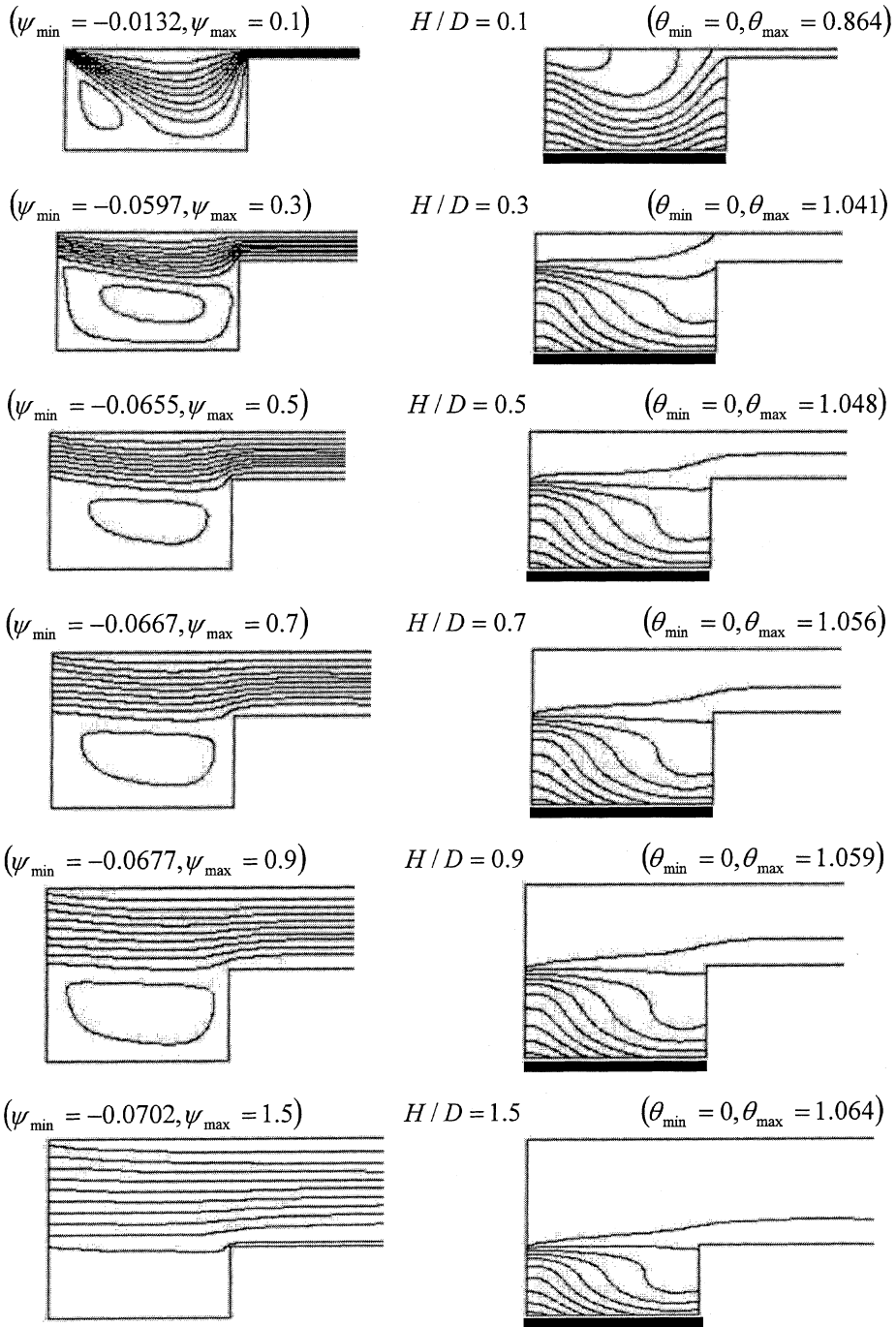


Figure 14. Streamlines and isotherms for heating from below at various  $H/D$  ( $Ri = 0.1, Re = 100$ ).

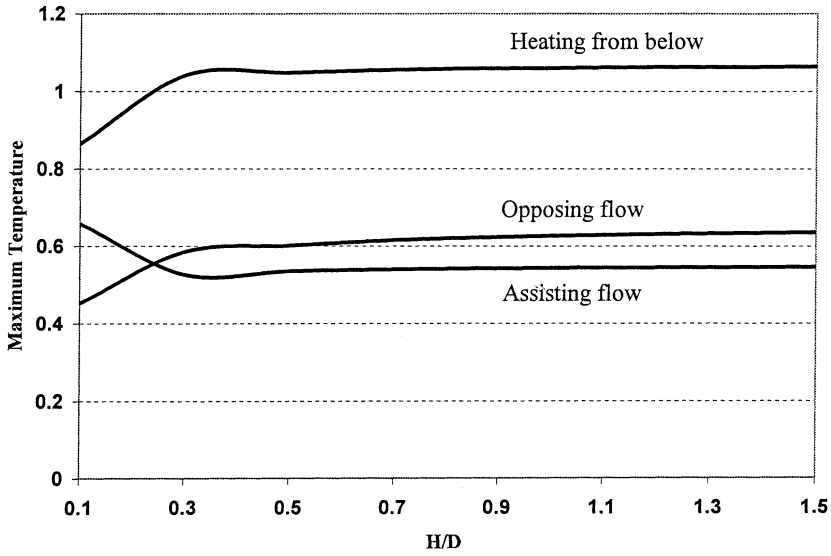


Figure 15. Comparison of the maximum temperature variation between assisting forced flow, opposing forced flow, and heating from below for various  $H/D$  ( $Ri = 0.1, Re = 100$ ).

figure shows that the opposing forced flow configuration has the highest average Nusselt number among other configurations. For an  $H/D$  ratio greater than 0.4, the average Nusselt number remains almost constant for all three configurations.

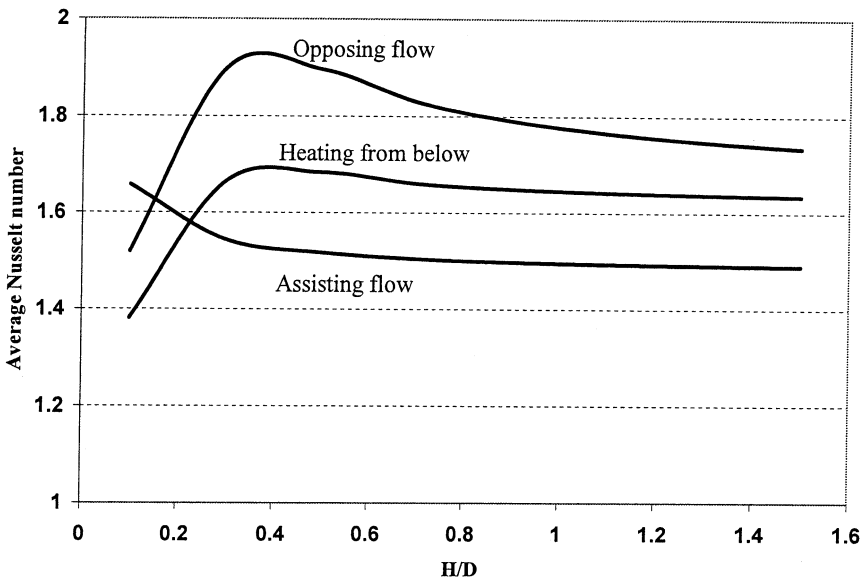


Figure 16. Comparison of the average Nusselt number between assisting forced flow, opposing forced flow, and heating from below for various  $H/D$  ( $Ri = 0.1, Re = 100$ ).

This again is due to the fact that the main bulk flow does not penetrate much inside the cavity.

### HEAT TRANSFER CORRELATIONS

The average Nusselt numbers shown in Figure 16 are correlated in terms of the ratio of the height of the inflow and outflow openings to the heat source length ( $H/D$ ) for a Richardson number of 0.1 and Reynolds number of 100. These correlations can be written as follows:

#### Assisting flow

$$\begin{aligned} \text{Nu} = & 1.6854 - 0.2164(H/D) - 1.933(H/D)^2 + 6.0347(H/D)^3 - 7.057(H/D)^4 \\ & + 3.7348(H/D)^5 - 0.74775(H/D)^6 \quad R^2 = 99\% \end{aligned} \quad (9)$$

Heating from below

$$\begin{aligned} \text{Nu} = & 1.0447 + 4.5323(H/D) - 12.366(H/D)^2 + 16.411(H/D)^3 - 11.39(H/D)^4 \\ & + 3.9545(H/D)^5 - 0.5379(H/D)^6 \quad R^2 = 99.9\% \end{aligned} \quad (10)$$

Opposing Flow

$$\begin{aligned} \text{Nu} = & 1.1093 + 5.0147(H/D) - 10.391(H/D)^2 + 6.9637(H/D)^3 + 1.5976(H/D)^4 \\ & - 3.5819(H/D)^5 + 1.0624(H/D)^6 \quad R^2 = 98.4\% \end{aligned} \quad (11)$$

where  $R^2$  is the maximum correlation coefficient.

### CONCLUSIONS

A numerical investigation on mixed convection in a partially open cavity (U-shaped) was carried out using a finite element analysis [18]. The results showed that there were marked differences among the three considered heating modes. For  $H/D = 1.0$  and a Reynolds numbers of 100 and 1000, it was noticed that recirculating cells develop within the cavity, which improve the heat removal from the heat source for the opposing case. For the assisting case, the results were similar to the ones presented in [13] for a heat source with a length shorter than the length of the cavity's vertical wall. The present results show that the opposing forced flow configuration has the highest average Nusselt number among other configurations for various  $H/D$ . In addition, the results of this investigation illustrate that the maximum temperature values decrease as the Reynolds and Richardson numbers increase for all three configurations. Generally, the highest thermal performance is achieved in the opposing mode.

## REFERENCES

1. M. Hasnaoui, E. Bilgen, and P. Vasseur, Natural Convection Above an Array of Open Cavities Heated from Below, *Numerical Heat Transfer, Part A*, vol. 18, pp. 463–482, 1990.
2. G. F. Jones and J. Cai, Analysis of a Transient Asymmetrically Heated/Cooled Open Thermosyphon, *J. Heat Transfer*, vol. 115, pp. 621–630, 1993.
3. R. A. Showole and J. D. Tarasuk, Experimental and Numerical Studies of Natural Convection with Flow Separation in Upward-Facing Inclined Open Cavities, *J. Heat Transfer*, vol. 115, pp. 592–605, 1993.
4. J. L. Lage, J. S. Lim, and A. Bejan, Natural Convection with Radiation in a Cavity with Open Top End, *J. Heat Transfer*, vol. 114, pp. 479–486, 1992.
5. A. A. Dehghan and M. Behnia, Combined Natural Convection-Conduction and Radiation Heat Transfer in a Discretely Heated Open Cavity, *J. Heat Transfer*, vol. 118, pp. 56–64, 1996.
6. P. H. Oosthuizen and J. T. Paul, Mixed Convective Heat Transfer in a Cavity, *ASME-HTD*, vol. 42, pp. 159–169, 1985.
7. J. P. Simoneau, C. Inard, and F. Allard, Numerical Approach of Interaction Between an Injection and Laminar Natural Convection in a Thermally Driven Cavity, *ASME-HTD*, vol. 99, pp. 45–51, 1988.
8. K. Vafai and J. Eftefagh, The Effects of Sharp Corners on Buoyancy-Driven Flows with Particular Emphasis on Outer Boundaries, *Int. J. Heat Mass Transfer*, vol. 33, pp. 2311–2328, 1990.
9. K. Vafai and J. Eftefagh, Thermal and Fluid Flow Instabilities in Buoyancy-Driven Flows in Open-Ended Cavities, *Int. J. Heat Mass Transfer*, vol. 33, pp. 2329–2344, 1990.
10. K. Vafai and J. Eftefagh, Axial Transport Effects on Natural Convection Inside of an Open Ended Annulus, *ASME J. Heat Transfer*, vol. 113, pp. 627–634, 1991.
11. K. Vafai, C. P. Desai, S. V. Iyer, and M. P. Dyko, Buoyancy Induced Convection in a Narrow Open-Ended Annulus, *ASME J. Heat Transfer*, vol. 119, pp. 483–494, 1997.
12. K. Khanafer and K. Vafai, Buoyancy-Driven Flow and Heat Transfer in Open-Ended Enclosures: Elimination of the Extended Boundaries, *Int. J. Heat Mass Transfer*, vol. 43, pp. 4087–4100, 2000.
13. E. Papanicolaou and Y. Jaluria, Mixed Convection from an Isolated Heat Source in a Rectangular Enclosure, *Numerical Heat Transfer, Part A*, vol. 18, pp. 427–461, 1990.
14. E. Papanicolaou and Y. Jaluria, Mixed Convection from a Localized Heat Source in a Cavity with Conducting Walls: A Numerical Study, *Numerical Heat Transfer, Part A*, vol. 23, pp. 463–484, 1993.
15. T. H. Hsu and S. G. Wang, Mixed Convection in a Rectangular Enclosure with Discrete Heat Sources, *Numerical Heat Transfer, Part A*, vol. 38, pp. 627–652, 2000.
16. C. Taylor and P. Hood, A Numerical Solution of the Navier-Stokes Equations Using Finite-Element Technique, *Comput. Fluids*, vol. 1, pp. 73–89, 1973.
17. P. M. Gresho, R. L. Lee, and R. L. Sani, On the Time-Dependent Solution of the Incompressible Navier-Stokes Equations in Two and Three Dimensions, In *Recent Advances in Numerical Methods in Fluids*, Pineridge, Swansea, UK, 1980.
18. *FIDAP Theoretical Manual*, Fluid Dynamics International, Evanston, IL, 1990.